Available online at www.sciencedirect.com

ScienceDirect

Procedia Engineering 10 (2011) 839–844

Engineering Procedia

ICM11

Creep behaviour and microstructure changes of model cast Ni-Cr-W-C alloys

Marie Kvapilova[a*], Kveta Kucharova[a], Vaclav Sklenicka[a], Milan Svoboda[a], Karel Hrbacek[b]

[a]*Institute of Physics of Materials, Academy of Sciences of the Czech Republic, CZ - 616 62 Brno, Czech Republic*
[b] *PBS Velka Bites, a.s., CZ - 592 12 Velka Bites, Czech Republic*

Abstract

A comparative study of creep and microstructural properties of two model cast Ni-Cr-W-C alloys (Alloys A and B) resistant to high-temperature oxidation with different contents of Cr, W, Zr and Fe was performed. Uniaxial tensile creep tests were carried out at temperatures from 1023 to 1273 K and at the applied stresses ranged from 20 to 250 MPa. Creep tests were followed by microstructural and fractographic investigations. A mutual comparison between the creep characteristics of the alloys under comparable creep loading conditions shows that the alloy B with higher contents of tungsten and zirconium is more creep resistant as that of the Alloy A at lower temperatures. It is suggested that the alloy A and B earn their creep strength from the combination of solid solution hardening and precipitation hardening. However, it is difficult to quantify each contribution to the overall creep strength. Possible reason for the different consequence of strengthening effects is discussed.

Keywords: cast Ni based superalloy, creep properties, creep strength, strengthening mechanism, microstructure, phase stability

1. Introduction

Various nickel-based superalloys have been developed for specific component applications in aerospace and power engineering industries. Most of the contemporary creep-resistant nickel based

* Corresponding author. Tel.:+420 532290374; fax: +420 541212301.
E-mail address: kvapilova@ipm.cz

Selection and peer-review under responsibility of ICM11 doi:10.1016/j.proeng.2011.04.138

superalloys owe their creep strength to fine and uniformly dispersed γ'- particles precipitating during ageing treatment following a solution annealing. However, nickel-based superalloys find widespread applications also in chemical industries. The choice for use of Ni-based superalloys in castings for extremely stressed components of glass industry facilities is primarily based on a good combination of creep rupture strength and ductility and resistance to high temperature oxidation for prolonged exposures. Thus, the as-cast Ni-Cr-W superalloys have been considered as potential high-temperature material for such applications [1].

Ni-Cr-W based superalloys that posses outstanding oxidation resistance have been developed for processing of specific components generally operating at high temperature and under very severe conditions. In those alloy systems the main strengthening mechanism is solid solution hardening which is provided by the refractory elements with high melting temperatures and low diffusivities such as W, Cr, Mo, Ta, Ru and Re [2]. However, excessive additions may render the alloys prone to high the formation of topologically close packed phases, which were shown to have deleterious effects on mechanical properties [3]. However, high content of carbon introduced into cast Ni-Cr-W superalloys may cause additional hardening by precipitation of carbides which is beneficial to creep properties [4]. The purpose of this paper is to describe the creep behaviour and the strengthening effects in two model cast Ni-Cr-W superalloys with different alloy chemistries.

2. Experimental materials and procedures

Two model alloys A and B were cast by a foundry company PBS Velká Bíteš, a.s., Czech Republic, using conical ingots with minimum diameter of 13 mm, maximum diameter of 18 mm and length of 90 mm. Their chemical compositions were as follows (in wt.%): **Alloy A**: Ni – 23.5 Cr, 14,9 Fe, 5.1 W, , 1.1 Si, 0.9 Mn, 0.3 C. **Alloy B**: Ni – 32.0 Cr, 7.4 W, 1.0 Si, 1.0 Zr, 1.0 Ta, 0.15 Mn, 0.1 Fe, 0.3 C. Both model alloys were investigated in their as-cast states. Standard uniaxial tensile creep tests were carried out using cylindrical creep specimens with gauge diameter of 3.5 mm and gauge length of 50 mm. The creep tests were performed at applied stresses ranging from 20 to 250 MPa and at temperatures from 1023 to 1273 K. The creep elongations were continuously measured using a linear variable differential transducer, recorded digitally and computer processed. All creep specimens were run to the final fracture. Following creep testing samples were prepared for microstructural examination by means of optical, scanning and transmission electron microscopy.

3. Results and Discussion

3.1. Creep tests at constant load and constant stress

Engineering tensile creep tests conducted at constant load are aimed at determination of the creep strength and/or creep fracture strength, i.e. the data needed for design. In this case, the load is related to the initial value of the applied stressσ. Creep tests performed at constant stress are frequently used in fundamental investigation of creep processes.

In Fig. 1 standard creep curves for the Alloys A and B are shown. The cross-section reduction of specimens remained quite uniform along the gauge length of the specimens almost up to fracture. It can be seen that in the constant-load tests the minimum creep rates higher than that at the constant stress. Further, at constant stress the times to fracture are considerably longer that those at constant load. Thus, creep tests at constant stresses running up to the final fracture are more time consuming than those at constant load. Constant load testing was used in what follows.

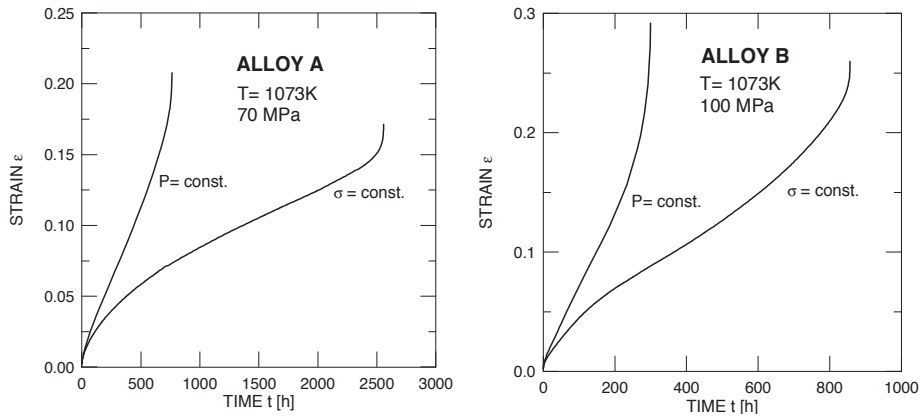

Fig. 1. Standard creep curves for constant load (P = const) and constant stress (σ = const) testing for (a) Alloy A, and (b) Alloy B.

3.2. Creep Results

In Figs. 2(a) and 3(a), the minimum creep rates $\dot{\varepsilon}_{min}$ of the Alloy A and B are plotted against the applied stress σ on a bilogarithmic scale. Examination of Figs. 2(a) and 3(a) leads to two observations. First, the minimum creep rates for the Alloy B are about one order of magnitude less than that for the Alloy A under the same loading conditions at lower temperatures. Second, it should be noted, that the stress dependences of $\dot{\varepsilon}_{min}$ for both alloys have same trend. However, the slopes and therefore the apparent stress exponents $n = (\partial \ln \dot{\varepsilon}_{min} / \partial \ln \sigma)_T$ for the Alloy A are slightly higher than those for the Alloy B. Further, for both alloys, the double logarithmic plots of the times to fracture t_f as a function of applied stress are shown in Figs. 2(b) and 3(b). It is clear from these plots that the creep lives of the Alloy B at lower temperatures are considerably longer than those of the Alloy A . The evaluated values of the stress exponent m of creep life ($t_f \propto B\sigma^{-m}$) are very similar to the values for stress exponent n. This could be explained by the fact, that both the creep deformation and fracture are controlled by the same mechanism(s).

The values of the strain to fracture in both alloys are shown in Fig. 4. Note that the creep ductility in the Alloy B is considerably increased at the highest testing temperatures.

3.3. Comparison of creep in Alloy A and Alloy B

As a proper characteristic of the creep strength, the flow stress σ_f causing a given minimum creep strain rate at a given temperature can be used for mutual comparison of the alloys [5]. In Tab. 1 the values of the flow stress as σ_f corresponding to the minimum creep strain rates 10^{-5}, 10^{-6}, 10^{-7} and 10^{-8} s^{-1} are shown for both the alloys considered. Inspection of Tab. 1 leads to two observations. First, the temperature dependences of the flow stress σ_f for both alloys are same in trend: as depicted in Tab. 1 the values of the flow stresses decrease strongly with increasing temperature. Second, the Alloy B exhibits a better creep strength than the Alloy A at lower temperature range. Up to 1173 K the values of the ratio $(\sigma_f(B) / \sigma_{f(A)}) > 1$. However, at temperatures T > 1173 K very small differences between $\sigma_{f(A)}$ and $\sigma_{f(B)}$ were found with a tendency to be $\sigma_{f(B)} / \sigma_{f(A)} < 1$ at the highest temperatures.

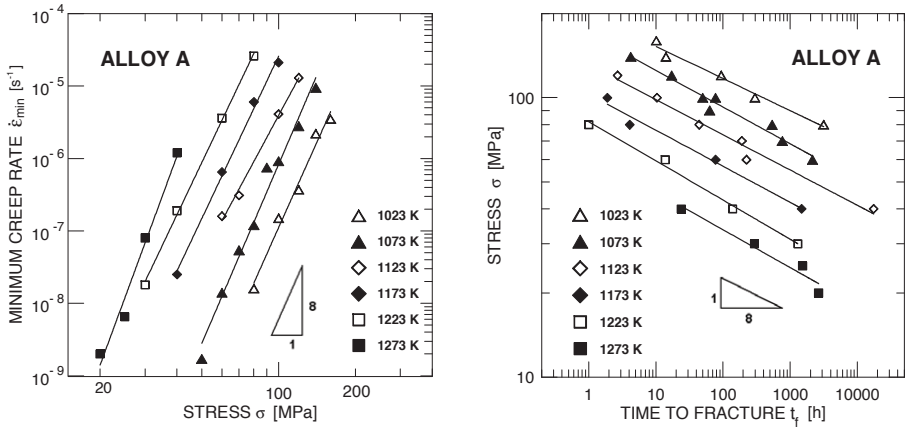

Fig. 2. Alloy A: stress dependence of (a) $\dot{\varepsilon}_{min}$ and (b) t_f.

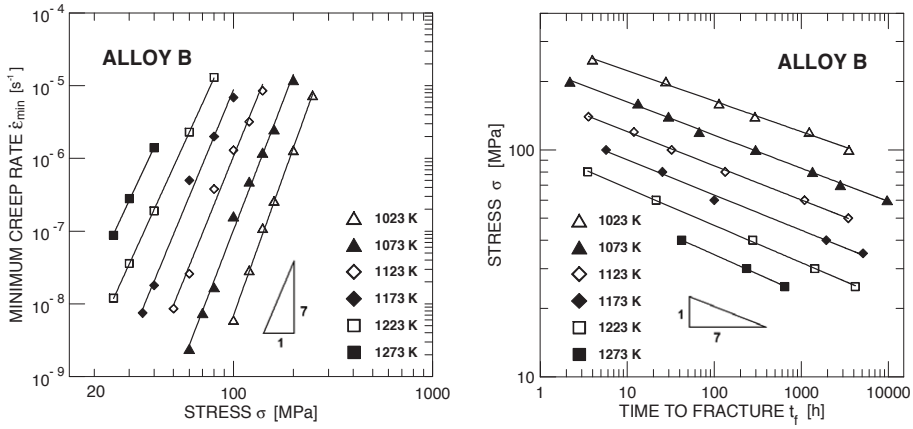

Fig. 3. Alloy B: stress dependence of (a) $\dot{\varepsilon}_{min}$ and (b) t_f.

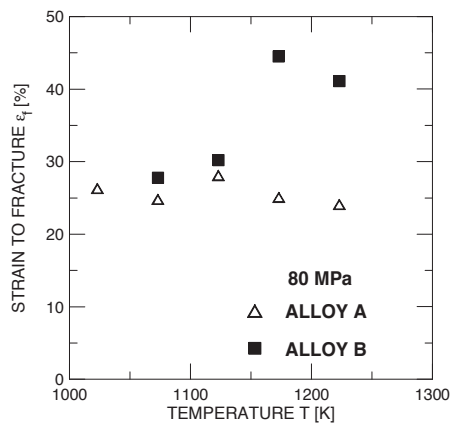

Fig. 4. Temperature dependence of strain to fracture ε_f.

Table 1. The values of the flow stresses $\sigma_{f(A)}$, $\sigma_{f(B)}$ and the rations $\sigma_{f(B)} / \sigma_{f(A)}$ for various minimum creep rates $\dot{\varepsilon}_{min}$.

	$\dot{\varepsilon}_{min} = 10^{-8}$ s^{-1}			$\dot{\varepsilon}_{min} = 10^{-7}$ s^{-1}			$\dot{\varepsilon}_{min} = 10^{-6}$ s^{-1}			$\dot{\varepsilon}_{min} = 10^{-5}$ s^{-1}		
T [K]	$\sigma_{f(A)}$ [MPa]	$\sigma_{f(B)}$ [MPa]	$\sigma_{f(B)}/\sigma_{f(A)}$	$\sigma_{f(A)}$ [MPa]	$\sigma_{f(B)}$ [MPa]	$\sigma_{f(B)}/\sigma_{f(A)}$	$\sigma_{f(A)}$ [MPa]	$\sigma_{f(B)}$ [MPa]	$\sigma_{f(B)}/\sigma_{f(A)}$	$\sigma_{f(A)}$ [MPa]	$\sigma_{f(B)}$ [MPa]	$\sigma_{f(B)}/\sigma_{f(A)}$
1023	73.7	104.9	1.42	98.7	141.7	1.44	132.3	191.5	1.45		258.7	
1073	58.4	72.1	1.23	77.3	99.6	1.29	102.4	137.6	1.34	135.5	190.1	1.40
1123		50.3		57.1	70.6	1.24	81.2	99.1	1.22	115.5	139.2	1.21
1173	34.8	35.9	1.03	47.4	50.8	1.07	64.6	72	1.11	88	102	1.16
1223	27.3	24.3	0.89	37.3	35.7	0.95	50.9	52.3	1.03	69.5	76.7	1.10
1273	24.5			31.2	25.4	0.81	39.7	37.6	0.95			

The evaluated values of the flow stresses $\sigma_{f(B)}$ and their ratio $\sigma_{f(B)} / \sigma_{f(A)}$ are similar in trend with experimentally determined stress dependences of the times to fracture t_f (Fig. 5). As is evident from Fig. 5(a), the Alloy B exhibits better creep resistance than the Alloy A at temperature of 1023 K; the values of the time to fraction for the Alloy B can be more than one order of magnitude longer than that of the Alloy B under the same loading conditions. This difference consistently decreases with increasing temperature, with a tendency at higher temperatures towards no effect of the type of the alloy chemistry on the lifetime. In fact, inspection of Fig. 5(b) reveals that at temperature of 1273 K the creep lives of the Alloy B seem to be essentially equal to that of the Alloy A.

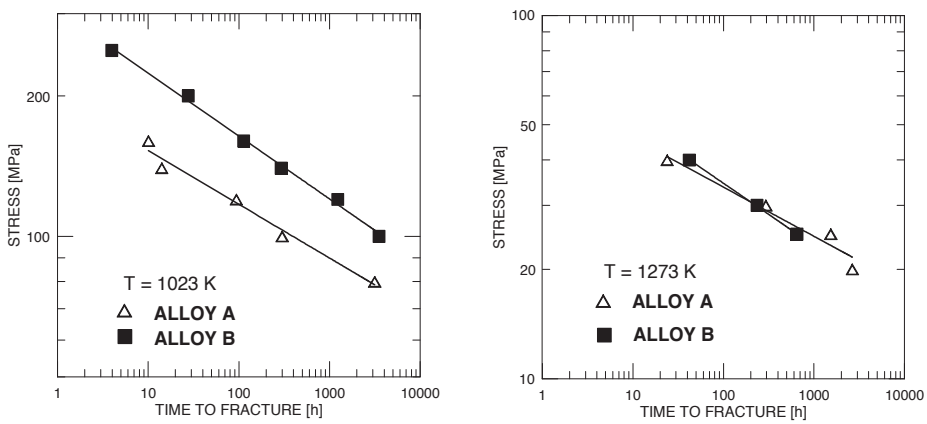

Fig. 5. Comparison of stress dependences of time of fracture of Alloys A and B at (a) 1023 K, and (b) 1273 K.

3.4. Microstructure and fractographic observations

Despite the fact that the chemical compositions of the Alloy A and B somewhat differ their microstructures formed during casting and creep exposures exhibit similar features. In addition to the fcc matrix, two main different precipitation phases were observed, namely complex carbides $M_{23}C_6$ type, (with M being essentially Cr, Fe, Ni and/or W) and M_6C (Cr, Ni, W, Fe, Ta, Nb, Zr). The vast majority was of the $M_{23}C_6$ type which appeared during casting as coarse-granular and blocky primary carbide particles decorating the interdendritic regions (Fig. 6). During long-term creep exposures especially at higher temperatures the amount of these primary carbides decreases due to their dissolution. More stable

precipitates seem to be primary carbides containing high content of tungsten in the Alloy B. Significant secondary discrete M_6C precipitation mostly situated in close proximity of interdendritic regions were observed in both of the alloys. This precipitation tends to be more intensive in the Alloy A at higher testing temperatures due to less stable primary carbides. Furthermore, in the Alloy B at temperatures up to 1123 K the intermetallic brittle topologically closed-packed phase with plate and/or needle-like morphology was observed (Fig. 6(a)). Its dissolution at the highest temperature (T >1123 K) could be connected with an increase of the fracture strain of the Alloy B (Fig. 3).

Transgranular mode of fracture was observed in the ruptured specimens of both alloys. Dimples nucleated at precipitates were seen on the fracture surfaces. It is expected that the same fracture mechanism most probably occurs in both alloys which is supported by very similar values of the stress exponent m of creep life (Fig. 2(b) and 3(b)).

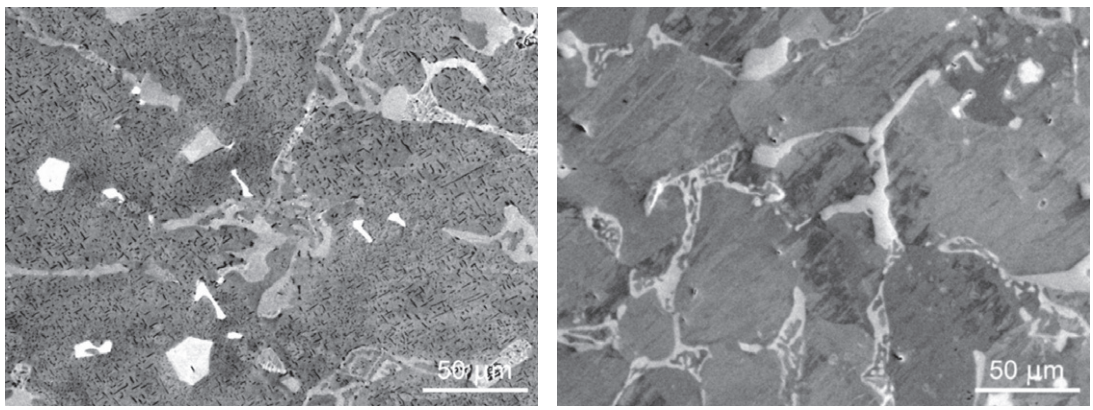

Fig. 6. Microstructure of Alloy B after creep at (a) 1023 K, and (b) 1273 K.

Acknowledgements

Financial support for this work was provided by the Ministry of Industry and Trade of the Czech Republic under the project FR-TI1/095 and the Academy of Science of the Czech Republic under the Research Plan No. AV0Z20410507.

References

[1] Liu Y, Li J, Kou H, Li H, Chamg H, Fu H. Hot working characteristic of as-cast and homogenized Ni-Cr-W superalloy. *Mater. Sci. Eng. A*, 2009, **508**, 141-7.

[2] Pollock T M, Tain S. Nickel-based superalloys for advanced turbine engines: chemistry, microstructure and properties. *J. Propeel. Power*. 2006, **22**, 361-74.

[3] Darolia R, Lahrman D F, Field R D. Formation of topologically closed packed phases in nickel base single crystal superalloys. In: Reichman S. et al., editors, *Superalloys 1998*, The Metalurgical Society: 1988, p. 255-264.

[4] Liu L R, Jin T, Zhao N R, Sun X F, Guan H R, Z. Q Hu. Formation of carbides and their effects on stress rupture of a Ni-base single crystal superalloys. *Mater. Sci. Eng. A,* 2003, **361**, 191-7.

[5] Cadek J, Pahutova M, Sustek V, Dlouhy A. On the role of recovery in creep of precipitation-strengthened polycrystalline nickel-base alloys. *Mater. Sci. Eng. A,* 1997, **238**, 391-8.